NANO LETTERS

2009
Vol. 9, No. 9
3124-3128

Effect of Stacking Order on the Electric-Field Induced Carrier Modulation in Graphene Bilayers

Adarsh Sagar,*,† Eduardo J. H. Lee,† Kannan Balasubramanian,† Marko Burghard,† and Klaus Kern†,‡

Max-Planck Institut fuer Festkoerperforschung, Heisenbergstrasse 1, D-70569 Stuttgart, Germany, and Institut de Physique de la Matière Condensée, Ecole Polytechnique Fédérale de Lausanne, CH-1015, Switzerland

Received April 15, 2009; Revised Manuscript Received June 19, 2009

ABSTRACT

When planar graphene sheets are stacked on top of each other, the electronic structure of the system varies with the position of the subsequent sublattice atoms. Here, we employ scanning photocurrent microscopy to study the disparity in the behavior of charge carriers for two different stacking configurations. It has been found that deviation from the regular Bernal stacking decouples the sheets from each other, which imparts effective electrostatic screening of the farther layer from the underlying backgate. Electrochemical top-gating is demonstrated as a means to selectively tune the charge carrier density in the decoupled upper layer.

Graphene's outstanding potential for applications in nanoelectronics has led to the development of intriguing prototype devices, including high frequency field-effect transistors,[1,2] single-electron transistors,[3] and spin valves.[4,5] However, there are several factors that hamper the performance of graphene-based devices, such as the relatively high conductivity minimum at the charge neutrality point, the sensitivity of charge transport against substrate inhomogeneities, and unwanted effects due to chemical adsorbates from the surrounding.[6,7] In this context, increasing attention has recently been directed to bilayer graphene which borrows physical properties from both single and few layer graphene. These include the possibility to tune its band gap by a perpendicular external electric field,[8,9] as well as a reduced level of electric potential fluctuations within the sheet.[10] So far, the fabrication of bilayer graphene has relied upon two major approaches, namely, mechanical exfoliation[11] and epitaxial growth on silicon carbide.[12]

Bilayer graphene usually exhibits crystalline ordering with an AB (Bernal) stacking, which eliminates the equivalence of sublattice carbon atoms in the individual layers, thereby distorting the linear inversion symmetry of the energy dispersion at the K point into parabolic bands.[13] The introduction of rotational stacking faults in such Bernal stacks results in misoriented stacking, whereupon the dispersion reverts back from parabolic to linear and thus a monolayer-like characteristic.[14] Experimentally, stacking misorientations in few-layer graphene have been observed both in epitaxially grown graphene and in micromechanically exfoliated graphene. In the latter case, misorientation results from the flipping of a flake extremity during mechanical exfoliation. While the effect of stacking order on the Raman properties of bilayer graphene has been studied in some detail,[15,16] only little is known regarding its electronic structure. Recent experiments using a dual gate configuration have enabled the independent control the charge carrier density in misoriented graphene

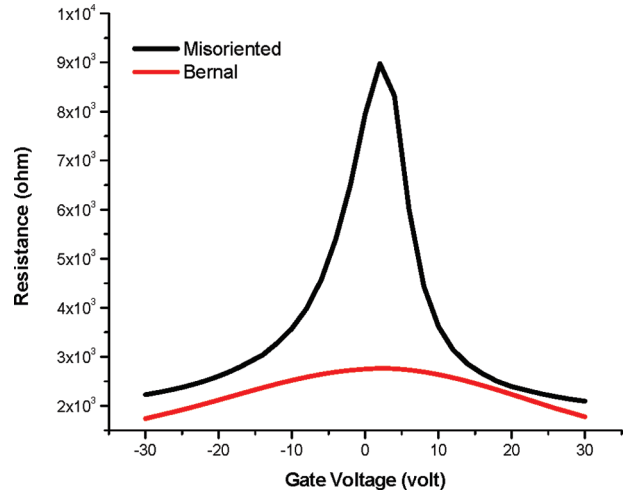

Figure 1. Plots of electrical resistance vs backgate voltage acquired from a misoriented (black curve) and a Bernal stacked (red curve) bilayer device at room temperature.

* Corresponding author. E-mail: a.sagar@fkf.mpg.de.
† Max-Planck Institut fuer Festkoerperforschung.
‡ Ecole Polytechnique Fédérale de Lausanne.

10.1021/nl9012002 CCC: $40.75
Published on Web 07/31/2009

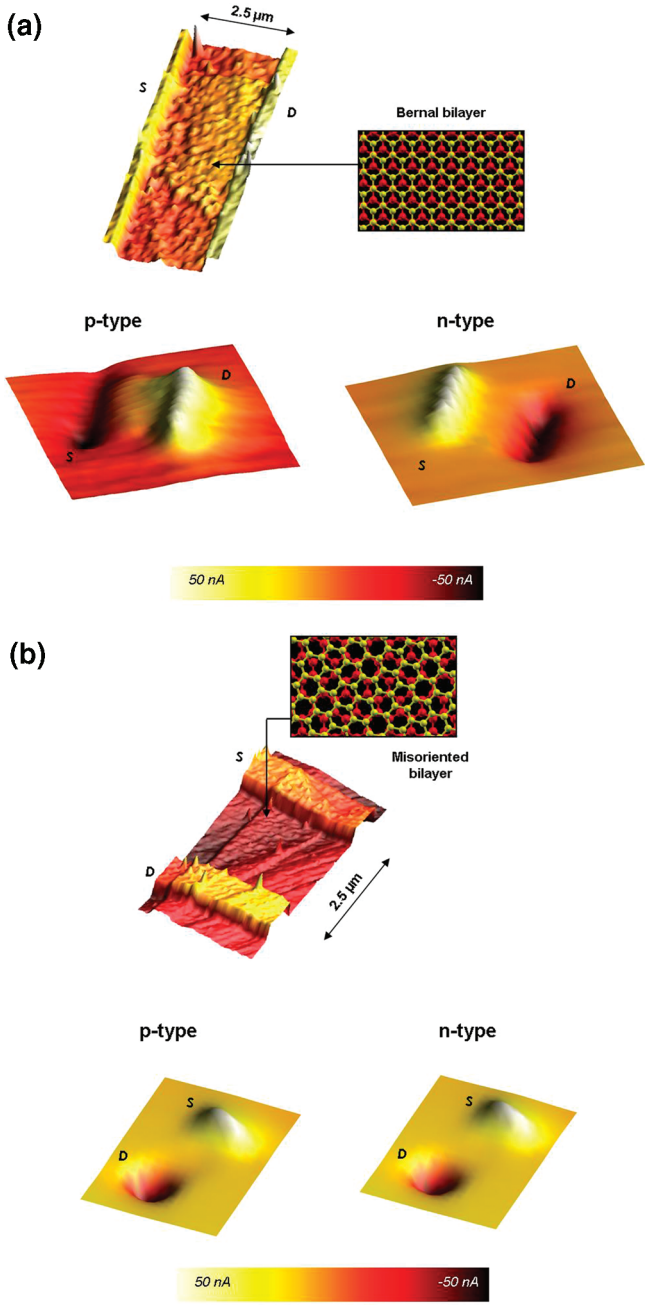

Figure 2. (a) AFM image of a Bernal stacked bilayer contacted with Ti/Au electrodes, where S is the source and D is the drain (top), and three-dimensional (3D) plots of the photocurrent responses of the device in the *p*- and *n*-type regimes (bottom). (b) AFM image of a misoriented bilayer device (top) and corresponding 3D plots of the photocurrent responses in the *p*- and *n*-type regimes (bottom).

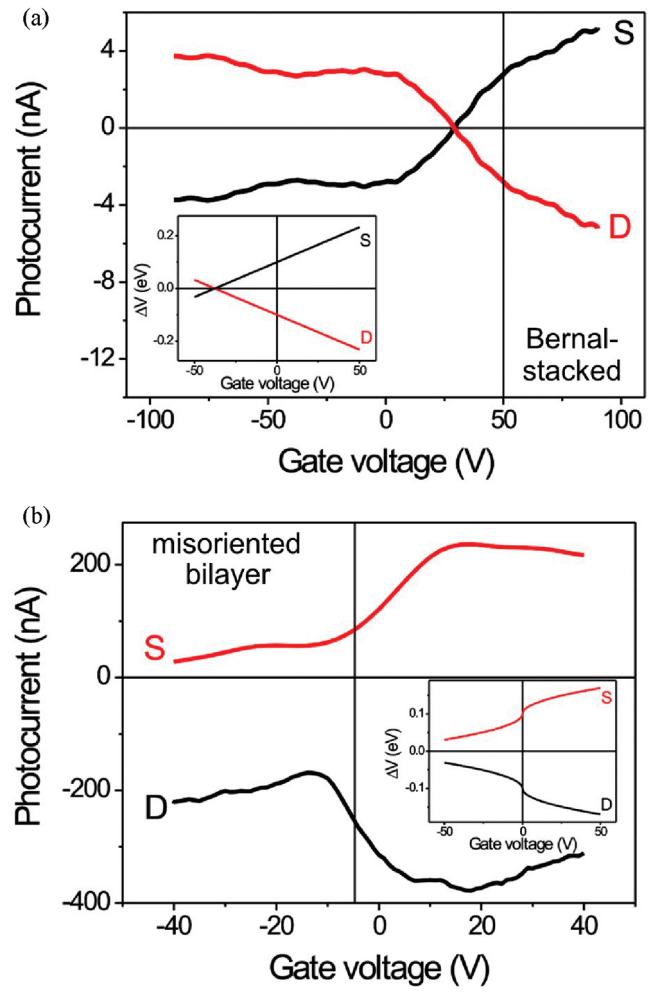

Figure 3. Comparison between experimental and calculated data obtained for the photocurrent responses at the contacts upon sweeping the back-gate voltages, with S and D respectively denoting source and drain in the devices. (a) In the Bernal stacked bilayer device, the signals invert polarity between the *p*- and *n*-type regimes. The inset shows the gate dependence calculated using eq 2 in the text. (b) The misoriented bilayer device does not show polarity inversion at the contacts. The inset depicts the dependence calculated based upon eq 3 in the text.

bilayers.[17] In this study, we use scanning photocurrent microscopy (SPCM) to monitor the changes in the potential landscape of the two different types of graphene bilayers upon application of a gate potential. The present results provide direct evidence for pronounced electrostatic shielding of the top layer within misoriented bilayer graphene. It is furthermore demonstrated that the carrier density in the top layer can be effectively modulated by means of electrochemical gating.

Bernal-stacked and misoriented bilayers were prepared by mechanical exfoliation of highly oriented pyrolytic graphite (HOPG) on Si substrates covered by 300 nm of thermally grown SiO_2. The two types of sheets were identified by optical microscopy and atomic force microscopy and then distinguished by Raman spectroscopy (Supporting Information Figure S1). Electrical contacts were defined by standard e-beam lithography, followed by evaporation of Ti (0.3 nm)/Au (15 nm) for the source and drain contacts. Among the 20 contacted bilayers a ratio of 5:3 was found between the Bernal-stacked and misoriented type. The degenerately doped Si substrate was used as a backgate during the electrical measurements performed under ambient. The transfer (resistance vs gate voltage) curves obtained from a Bernal-type and a misoriented bilayer sample are depicted in Figure 1. While in both cases ambipolar behavior is observed, the Bernal-stacked sample exhibits a broad minimum conductance which can be attributed to the chemical interaction with

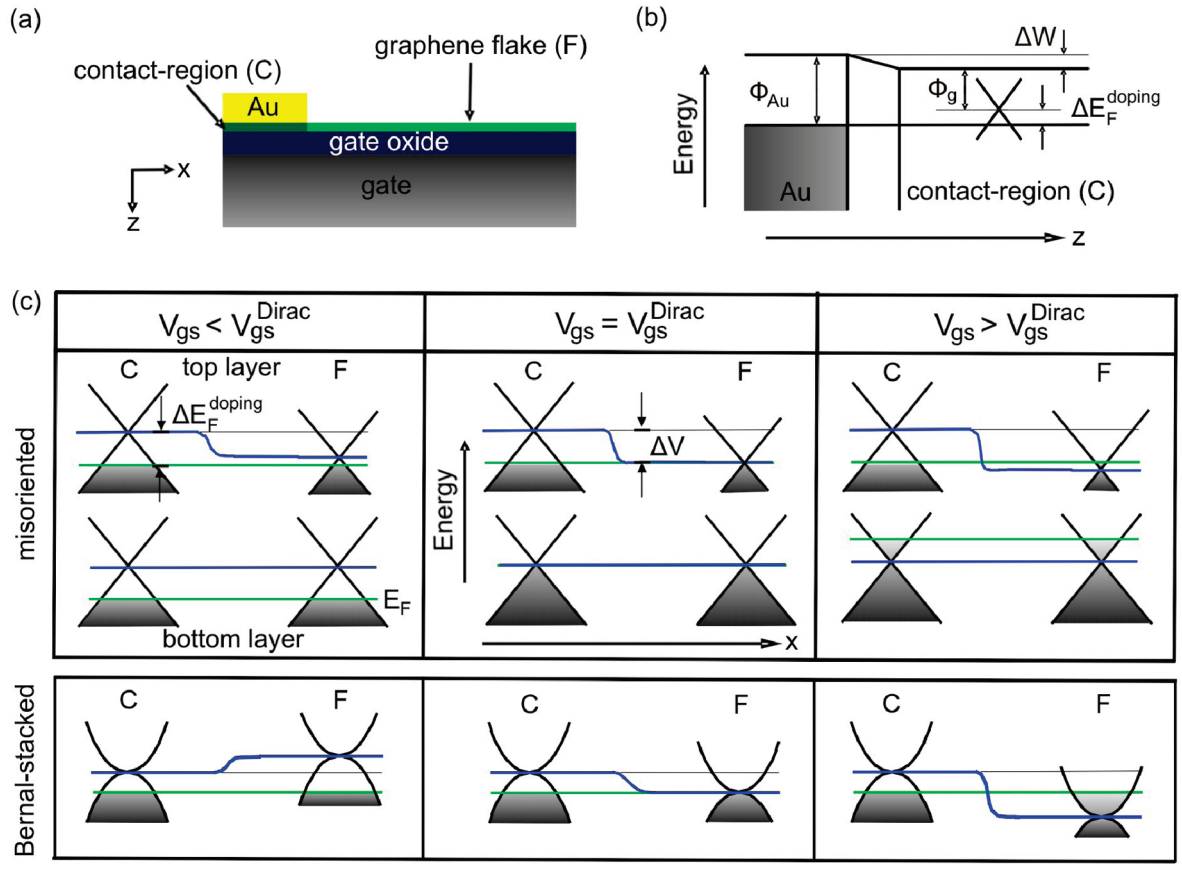

Figure 4. (a) Schematic cross-section of a bilayer graphene device, wherein the graphene region underneath the electrical contacts is denoted as contact region graphene C, and the device channel is referred to as flake F. (b) An energy band diagram of the device. (c) Schematic representation of the potential profile changes induced by back-gating in the two types of devices.

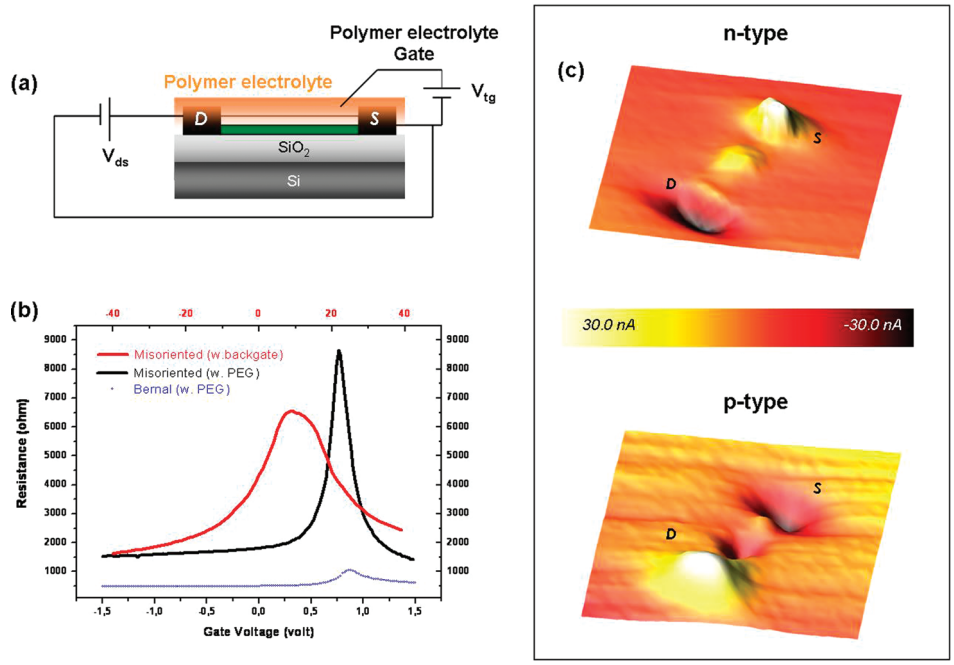

Figure 5. (a) A schematic cross-section of an electrochemically top-gated bilayer graphene device. (b) Comparative plots of the resistance vs gate voltage for the two types of bilayers devices in top-gated confuguration. (c) Three-dimensional plots of photocurrent generated in the top-gated misoriented bilayer device and Bernal-stacked device in the *p*- and *n*-type regimes.

the underlying substrate.[6] By contrast, the measured gate dependent resistance of a misoriented bilayer device closely resembles the response of monolayer graphene devices, featuring a narrow transition from the *p*- to the *n*-type regimes. This finding is consistent with theoretical and experimental studies, according to which misoriented bilayers

retain the linear energy dispersion of monolayer graphene and the two monolayers behave as electrically independent systems contacted in parallel.[18] As a consequence, the backgate dependent electrical transport characteristic is dominated by the bottom layer, wherein the carrier density is roughly seven times larger than in the top layer.[17]

In order to determine the potential profiles in the two types of devices as a function of the backgate potential, we used scanning photocurrent microscopy (SPCM). This technique has previously been applied to evaluate the electrostatic potential distribution in carbon nanotube[19,20] and monolayer graphene devices.[21,22] In SPCM, photocurrent signals are generated due to the dissociation of photoexcited electron−hole pairs in regions where local electric fields are present. The SPCM measurements were carried out by recording the short-circuit photocurrent generated through local illumination by a diffraction-limited laser spot (~400 nm diameter, $\lambda = 514.5$ nm, power ~100 kW cm^{-2}). Reflection images were recorded simultaneously during raster-scanning to correlate the origin of the photoresponses to actual positions within the devices. All SPCM data were acquired under ambient conditions.

Figure 2a shows the AFM image and the corresponding zero-bias photocurrent maps of a Bernal stacked bilayer in the *p*- and *n*-type transport regimes. It is apparent that the photocurrent response is dominated by strong signals located around the electrode edges. These signals invert polarity when the devices are switched from the *p*- to the *n*-type regime. Such behavior is similar to that previously reported for monolayer graphene devices and can be attributed to gate-dependent potential steps at the metal/graphene interfaces.[21] By contrast, the photocurrent signals close to the contacts in misoriented bilayer devices (figure 2b) are only weakly affected by the backgate voltage (V_{gs}); in particular they do not invert sign even in high carrier density regimes, ~30 V away from minimum conductance voltages. To understand the origin of this difference, we compare the experimental back-gate modulated photocurrent responses at the contacts with model calculations based upon the respective dispersion relations expected for the two types of bilayers. The photocurrents measured while the laser spot was fixed directly at the metal/graphene interfaces are plotted in figure 3 against the applied back-gate voltage. In close correspondence to the photocurrent maps in Figure 2, the contact signals in the Bernal-stacked device are seen to invert the sign upon gate modulation, whereas no such change occurs in the misoriented bilayer device. Figure 4a displays the schematic cross-section of a bilayer graphene device, wherein the graphene region underneath the electrical contacts is denoted as contact region graphene (C) and the device channel is referred to as flake (F). According to theory, the difference between the work functions of the metal (Φ_m) and graphene (Φ_g) leads to charge transfer at the contact region, associated with a shift of the Fermi level with respect to the Dirac point (ΔE_F^{doping}),[23] as depicted in Figure 4b. It has furthermore been demonstrated that Au contacts *p*-dope the underlying contact region, where the charge carrier concentration *n* remains largely unaffected by the gate.[22] Thus, a potential step (ΔV) results at the interface between the contact region (C) and the device channel (F), whose magnitude is strongly dependent on the carrier density in the channel, which obeys the relation $n = \alpha V_{gs}$ (α being the gate coupling parameter). Accordingly, the gate dependent potential step can be generally expressed by

$$\Delta V = -\Delta E_F^{doping} - f(V_{gs}) = -(\Phi_m - \Phi_g - \Delta W) - f(V_{gs}) \quad (1)$$

where $f(V_{gs})$ represents the electrostatic doping Fermi level shift in the graphene channel as a function of the gate voltage and ΔW is the potential step at the interface between the metal contacts and the underlying graphene.

On the basis of eq 1, the experimentally determined back-gate modulation of the contact potential step ΔV can be predicted for both types of bilayers. For the Bernal-stacked graphene bilayer, insertion of the parabolic energy dispersion $E_k = \pm\hbar^2k^2/2m^*$, with the effective mass $m^* = 0.033m_e$ and $k_F = \sqrt{(\pi n)}$, yields the following relation for the potential step:

$$\Delta V = -\Delta E_F^{doping} - \frac{\pi\hbar^2}{2m^*}\alpha(V_{gs} - V_{gs}^{Dirac}) \quad (2)$$

where $\alpha = 7.3 \times 10^{10}$ cm^{-2} V^{-1}.[24] The corresponding linear plots obtained with $\Phi_m = 4.7$ eV, $\Phi_g = 4.5$ eV, and $\Delta E_F^{doping} = 0.1$ eV agree well with the measured data (see inset Figure 3a), except for the high carrier concentration regimes, where the experimental curves show photocurrent saturation that generally occurs for high electric fields at metal−semiconductor junctions[25] due to the exhaustion of photoexcited charge carriers. The overall gate-induced changes are schematically illustrated in Figure 4c (bottom panel), from which it is apparent that a negative gate voltage is able to balance the carrier concentration between the contact and the channel, thereby inverting the negative contact potential steps at the Dirac point. In case of the misoriented bilayers, agreement between the potential step model and the experimental data requires assuming that due to decoupling of the layers, only the top layer experiences metal contact doping (Figure 4c, top panel). In this manner, the contact region graphene in the bottom layer remains unaffected by the metal contacts, and consequently its carrier density varies together with that of the graphene channel. The contact potential step then mostly resides within the top layer, which can be similarly described as in monolayer graphene devices. To take into account that screening by the bottom layer should reduce the electrostatic coupling of the backgate, an effective gate coupling parameter α_{eff} is included in the relation for the potential step within the top layer:

$$\Delta V = -\Delta E_F^{doping} - \mathrm{sgn}(V_{gs} - V_{gs}^{Dirac})\hbar|v_F|\sqrt{\pi\alpha_{eff}}\sqrt{V_{gs} - V_{gs}^{Dirac}} \quad (3)$$

For further evaluation, we use $\alpha_{eff} = 1 \times 10^{10}$ cm^{-2} V^{-1}, a value obtained by fitting the experimental results of ref 17

with the relation $n = \alpha V_{gs}$. Thus gained plots (inset of Figure 3b) reproduce the measured curves, including the absence of sign inversion of the potential step, and display a significantly slower modulation compared to the Bernal-stacked bilayers when all other parameters are kept constant.

The electronic decoupling of misoriented bilayer graphene provides a suitable basis for independently controlling the charge carrier density within the layer farther from the substrate. We addressed this task by applying a polymer electrolyte gate consisting of PEO and $LiClO_4$: 20 mg/mL polyethyleneoxide, 10 mg/mL lithium perchlorate in a mixture of methanol/water (v/v 4:1) on top of the conducting channel (Figure 5a), following a previously established approach for other carbon based devices.[26,27] Compared to the Si backgate, the polymer electrolyte gating yields a considerably improved transconductance, as apparent from the transfer characteristics compared in Figure 5b. For instance, only a rather narrow gate voltage range of ~1.5 V is needed to switch the misoriented bilayer device from the *n*- to the *p*-type regime, with a high I_{ON}/I_{OFF} ratio of ~10. This ratio is much lower in case of the Bernal-stacked bilayer, in close correspondence to the back gate action (Figure 1). That the charge carrier density of the top layer in the misoriented bilayers can indeed be modulated by the electrochemical gate is confirmed by the sign inversion of the contact photocurrent responses observed in this gating configuration (Figure 5c), thus further corroborating the model in Figure 4c. The photocurrent images also reveal photocurrent fluctuations on the sheets, which were absent prior to the polymer deposition. These features most likely originate from charge impurities contained in the polymer electrolyte topgate. As a consequence of their single-crystalline character, Bernal bilayer devices show a similar SPCM response like under back-gating (see Supporting Information).

In summary, the presented SPCM data directly proves that the layers in misoriented bilayer graphene are electronically decoupled from each other as a result of their rotational stacking fault, in stark contrast to Bernal-stacked bilayers, which behave as single crystals. The bottom layer in the first type of material acts like a pseudo-substrate providing electrostatic screening of the top layer from the substrate, which may be exploited for the development of novel, high performance field-effect devices.

Acknowledgment. The authors would like to thank Giacomo Levita for his help with the structural diagrams of the bilayers. WSxM software[28] was used to plot the photocurrent responses obtained.

Supporting Information Available: Raman spectra of the two types of bilayer graphene, measured at 633 nm excitation. Photocurrent measurements of Bernal bilayers in electrochemical top-gated configuration, including an AFM image of the sample before the top-gate configuration. Comparative plots of the calculated carrier mobilities for the top-gated configurations. This material is available free of charge via the Internet at http://pubs.acs.org.

References

(1) Chen, Z.; Lin, Y. M.; Rooks, M. J.; Avouris, P. *Physica E* **2007**, *40*, 228.
(2) Echtermeyer, T. J.; Lemme, M. C.; Baus, M.; Szafrenek, B. N.; Geim, A. K. *IEEE Device Lett.* **2008**, *29*, 952.
(3) Ponomarenko, L. A.; Schedin, F.; Katsnelson, M. I.; Yang, R.; Hill, E. W.; Novoselov, K. S.; Geim, A. K. *Science* **2008**, *320*, 356.
(4) Son, Y. W.; Cohen, M. L.; Louie, S. G. *Nature* **2006**, *444*, 347.
(5) Yokoyama, T. *Phy. Rev. B* **2006**, *77*, 073413.
(6) Shemella, P.; Nayak, S. K. *Appl. Phy. Lett.* **2009**, *94*, 032101.
(7) Zhou, S. Y.; Gweon, G.-H.; Fedorov, A. V.; First, P. N.; De Heer, W. A.; Lee, D.-H.; Guinea, F.; Castro Neto, A. H.; Lanzara, A. *Nat. Mater.* **2007**, *6*, 916.
(8) Castro, E. V.; Novoselov, K. S.; Morozov, S. V.; Peres, N. M. R.; Dos Santos, J.; Lopes, B.; Nilsson, J.; Guinea, F.; Geim, A. K.; Neto, A. H. C. *Phys. Rev. Lett.* **2007**, *99*, 216802.
(9) Oostinga, J. B.; Heersche, H. B.; Liu, X.; Morpurgo, A. F.; Vandersypen, L. M. K. *Nat. Mater.* **2008**, *17*, 151.
(10) Lin, Y.-M.; Avouris, P. *Nano Lett.* **2008**, *8*, 8.
(11) Novoselov, K. S.; Geim, A. K.; Morozov, S. V.; Jiang, D.; Zhang, Y.; Dubonos, S. V.; Grigorieva, I. V.; Firsov, A. A. *Science* **2004**, *306*, 666.
(12) Berger, C.; Song, Z. M.; Li, T. B.; Li, X. B.; Ogbazghi, A. Y.; Feng, R.; Dai, Z. T.; Marchenkov, A. N.; Conrad, E. H.; First, P. N.; de Heer, W. A. *J. Phys. Chem. B* **2004**, *108*, 19912.
(13) McCann, E.; Kechedzhi, K.; Fal'ko, Vladimir, I.; Suzuura, H.; Ando, T.; Altshuler, B. L. *Phys. Rev. Lett.* **2006**, *96*, 086805.
(14) Latil, S.; Henrad, L. *Phys. Rev. Lett.* **2006**, *97*, 036803.
(15) Poncharal, P.; Ayari, A.; Michel, T.; Sauvajol, J.-L. *Phys. Rev. Lett.* **2008**, *78*, 113407.
(16) Malard, L. M.; Nilsson, J.; Elias, D. C.; Brant, J. C.; Plentz, F.; Alves, E. S.; Castro Neto, A.H. ; Pimenta, M. A. *Phys. Rev. Lett.* **2007**, *76*, 201401.
(17) Schmidt, H.; Luedtke, T.; Barthold, P.; McCann, E.; Fal'ko, V. I.; Haug, R. J. *Appl. Phy. Lett.* **2008**, *93*, 172108.
(18) Gruenis, A.; Attaccalite, C.; Pichler, T.; Zabolotnyy, V.; Shiozawa, H.; Molodtsov, S. L.; Inosov, D.; Koitzsch, A.; Knupfer, M.; Schiessling, J.; Follath, R.; Weber, R.; Rudolf, P.; Wirtz, L.; Rubio, A. *Phys. Rev. Lett.* **2008**, *100*, 037601.
(19) Balasubramanian, K.; Fan, Y.; Burghard, M.; Kern, K.; Friedrich, M.; Wannek, U.; Mews, A. *Appl. Phy. Lett.* **2004**, *84*, 2400.
(20) Lee, E. J. H.; Balasubramanian, K.; Fu, N.; Dorfmüller, J.; Vogelgesang, R.; Mews, A.; Burghard, M.; Kern, K. *Small* **2007**, *3*, 2038.
(21) Lee, E. J. H.; Balasubramanian, K.; Weitz, R. T.; Burghard, M.; Kern, K *Nat. Nanotech.* **2008**, *3*, 486.
(22) Xia, F.; Mueller, T.; Golizadeh-Mojarad, R.; Freitag, M.; Lin, Y.; Tsang, J.; Perebeinos, V.; Avouris, P. *Nano Lett.* **2009**, *9*, 1039.
(23) Giovannetti, G.; Khomyakov, P. A.; Brocks, G.; Karpan, V. M.; van den Brink, J.; Kelly, P. J. *Phys. Rev. Lett.* **2008**, *101*, 026803.
(24) Novoselov, K. S.; McCann, E.; Morozov, S. V.; Fal'ko, V. I.; Katsnelson, M. I.; Zeitler, U.; Jiang, D.; Schedin, F.; Geim, A. K. *Nat. Phys.* **2006**, *2*, 177.
(25) Gu, Y.; Kwak, E.-S.; Lensch, J. L.; Allen, J. E.; Odom, T. W.; Lauhon, L. J. *Appl. Phy. Lett.* **2005**, *87*, 043111.
(26) Das, A.; Pisana, S.; Chakraborty, B.; Piscanec, S.; Saha, S. K.; Waghmare, U. V.; Novoselov, K. S.; Krishnamurthy, H. R.; Geim, A. K.; Ferrari, A. C.; Sood, A. K. *Nat. Nanotech.* **2008**, *3*, 210.
(27) Balasubramanian, K.; Lee, E. J. H.; Weitz, R. T.; Burghard, M.; Kern, K. *Phys. Status Solidi A* **2008**, *205*, 633.
(28) Horcas, I.; Fernandez, R.; Gomez-Rodriguez, J. M.; Colchero, J.; Gomez-Herrero, J.; Baro, A. M. *Rev. Sci. Instrum.* **2007**, *78*, 013705.

NL9012002